ACS APPLIED MATERIALS & INTERFACES

www.acsami.org

Research Article

Nano-Filamented Textile Sensor Platform with High Structure Sensitivity

Shan Yan, Dong K. Dinh, Guojung Shang, Shan Wang, Wei Zhao, Xin Liu, Richard Robinson, Jack P. Lombardi, III, Ning He, Susan Lu, Mark Poliks, Benjamin S. Hsiao, Ivan Gitsov, and Chuan-Jian Zhong*

Cite This: *ACS Appl. Mater. Interfaces* 2022, 14, 15391−15400

Read Online

ACCESS | Metrics & More | Article Recommendations | Supporting Information

ABSTRACT: A key challenge to the creation of chemically responsive electro-functionality of nonconductive, hydrophobic, and free-contacted textile or fibrous network materials is how to impart the 3D structure with functional filaments to enable responsive structure sensitivity, which is critical in establishing the fibrous platform technology for sensor applications. We demonstrate this capability using an electrospun polymeric fibrous substrate embedded with nano-filaments defined by size-tunable gold nanoparticles and structurally sensitive dendrons as crosslinkers. The resulting interparticle properties strongly depend on the assembly of the nano-filaments, enabling an interface with high structure sensitivity to molecular interactions. This is demonstrated with chemiresistive responses to vaporous alcohol molecules with different chain lengths and isomers, which is critical in breath and sweat sensing involving a high-moisture or -humidity background. The sensitivity scales with the chain length and varies with their isomers. This approach harnesses the multifunctional tunability of the nano-filaments in a sensor array format, showing high structure sensitivity to the alcohol molecules with different chain lengths and isomers. The high structure sensitivity and its implications for a paradigm shift in the design of textile sensor arrays for multiplexing human performance monitoring via breath or sweat sensing and environmental monitoring of air quality are also discussed.

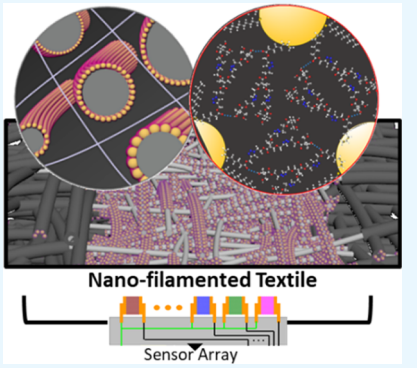

KEYWORDS: *nano-filaments, electrospun networks, structure sensitivities, dendron assemblies, sensor arrays*

1. INTRODUCTION

Fibrous or textile materials used in various applications often require assembly and interlacing of fibers to translate one-dimensional (1D) structures into two-dimensional (2D)/three-dimensional (3D) structures where the internal structure and component interaction of individual fibers define the physical and chemical properties.[1] Imparting such materials with responsive functions could lead to four-dimensional (4D) textiles, which may be achieved by additive manufacturing[2,3] and surface-functionalized 3D printing.[4] Currently, there is little knowledge on how such functionalization can be established inside the fibrous, porous, and interlaced textiles so that the unique interlocking or interlacing of the network of fibers can be effectively exploited for interweaving in a 3D manner to form a web or porous structure to harness the microelectronics, sensors, and biosensors for energy production, storage, and conversion via the mechanically, thermally, or chemically entangling fibers or filaments. Such fibrous structures allow tunability of porosity, wettability, permeability, dense or loose bundling/flocking, and rigid or soft networking.[5] In contrast to cellulose with a sugar backbone, dense bundling, and strong hydrophilic characters, which are sometimes problematic for applications requiring minimization of a moisture-dominant background (e.g., sweat and breath sensors), electrospun nanofibers with a synthetic polymeric backbone, tunable rigidity, flocking, networking, and hydrophilicity/hydrophobicity present a highly diversified opportunity for applications involving a high-humidity background.[6] A key challenge is the ability to controllably fabricate the textile substrates with a combination of nano-filaments and polymer fibers with intertwined, interweaved, or free-contacted structures (Scheme S1).

We demonstrate herein a new strategy for fabricating a nano-filamented textile sensor platform by imparting the electrospun fiber network with electrical conductivity and chemical functionality. The tunable porosity and hydrophilicity of interlaced electrospun polymer fibers and nano-filaments create a network with the desired sensing properties in a flexible, low-cost, and disposable paper-like substrate format. In the context of 1D−2D−3D−4D fibrous materials for the chemiresistor sensor application described in this report, 1D refers to

Received: January 1, 2022
Accepted: March 8, 2022
Published: March 25, 2022

Scheme 1. (a) Illustration of the 3D Fibrous Textile Sensor Interface; (b) Illustration of the Functionalized Au NP-Coated Fibers as a Sensitive Filament and Carbon-Coated Fibers as a Conductive Filament; (c) Illustration of Tunability of the Sensitive Filaments in Terms of Au NP and Fiber Sizes; (d) Illustration of the Tunable Sensitive Filament in Terms of Interparticle Ligands and Linkers; and (e) Illustration of a Chemiresistor Sensor Array (DD Stands for Dendrons; NDT Stands for 1,9-Nonanedithiol, and DT Stands for Decanethiol)

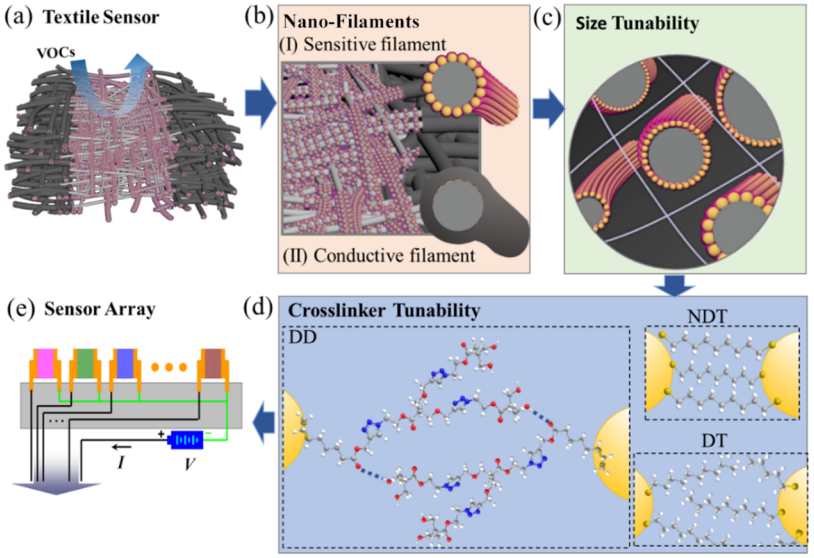

individual fibers in this work. 2D refers to a structure in the *XY* plane assembled by the 1D fibers. 3D is defined as the framework assembled by the fibers in the *XYZ* space. 4D refers to a textile structure that can change shape or function over time upon the influence of a stimulus, which in this work is the nanoparticle-filamented textile framework in which the fiber-anchored interparticle distances and strains respond to the adsorption of analytes, leading to electro-response functionality. While polymer materials have attracted a great deal of interest in paper electronics, wearable sensors, and energy storages,[7,8] including our own recent work,[9−15] few have demonstrated the tunability of 1D−2D−3D−4D assemblies in combination with the nano-filaments other than 3D printing. The nano-filament-functionalized fibrous network provides an ideal platform for environmental sensing and healthcare monitoring.[16−20] Fibrous papers have been exploited for flexible, foldable, biocompatible, biodegradable, disposable, inexpensive, and wearable sensors.[21−23] Fibrous networks with nanoparticles are explored as building blocks for electrochemical sensors, strain sensors, and biosensors[24,25] for environmental monitoring of air quality and human breath/sweat monitoring of disease-related biomarkers.[9,26−28] Earlier examples include deposition of gold nanoparticles (Au NPs) in paper as surface-enhanced Raman spectroscopy substrates,[29] electrodeposition of the Au nanostructure on paper as a glucose sensor,[30] in situ growth of Au NPs on polyacrylonitrile (PAN) fibers for an electrochemiluminescence sensor,[31] in situ growth of Cu NPs on fabrics for heating,[32] growth of Ag@Si NPs on a fibrous structure for fluorescence biosensing,[33] sputtering Pd on filtration paper for hydrogen sensing,[34] and the nanoparticle fibrous membrane for volatile organic compound (VOC) detection.[12] However, most of the fibrous substrates reported for sensor applications are dense networks with smaller porosity and lower permeability (e.g., cellulose), which are easily saturated by adsorbed molecules, especially in breath and sweet sensing where there is a large amount of water moisture in the background. In comparison with the dense networks, loose networks with relatively rigid fibers feature large porosity and high permeability that allow molecules to transfer faster to avoid saturation.[35] This attribute provides increased tunability of sensitivity and selectivity for breath sensing of VOC biomarkers of lung cancer.[36] Alcohols are one of the major VOC groups in lung cancer breath (e.g., 2-ethyl-1-hexanol, 2-ethyl-4-methyl-1-pentanol, and 2-propyl-1-pentanol). It is challenging to detect alcohols of different chain lengths and isomers. The most reliable detection of blood alcohol content levels involves blood sampling or urine monitoring, which are invasive or time-consuming.[37] Saliva, breath, and sweat samples are convenient for noninvasive and real-time alcohol detection. Some of the reported sensors include 2D photonic crystals,[38] a titanium dioxide composite, or graphite-doped hydroxyapatite nanoceramics[39,40] for sensing methanol, ethanol, propanol, butanol, and propanol. However, many of the earlier sensors could suffer from a high false-positive rate due to the interference of the high moisture content and other compounds in the samples. Currently, none of the noninvasive sensors, including commercial ones, have shown the ability for sensing alcohols with different chain lengths and isomers, which is critical in applications involving breath and sweat sensors.

In contrast to the sensors built with densely bundled and strongly hydrophilic cellulose,[10−12] the high structure sensitivity demonstrated in this work harnesses the nano-filaments consisting of structurally sensitive dendrons and size-tunable Au NPs in an electrospun polymeric fiber network with tunable rigidity, flocking, and hydrophobicity (Scheme 1). We demonstrate that the response characteristics of chemiresistive sensors on the fibrous platform are tunable by manipulating the size of the dendronized Au NPs and the size of the fibers within the fibrous microstructure. This strategy enables the ability to introduce functionalities in terms of conductive and sensitive filaments. Dendron-mediated Au NP assemblies on fibrous substrates with different diameters are explored, where the functionalization with dendrons introduces a combination of hydrophobic, hydrophilic, and dielectric microenvironments for

https://doi.org/10.1021/acsami.2c00021
ACS Appl. Mater. Interfaces 2022, 14, 15391−15400

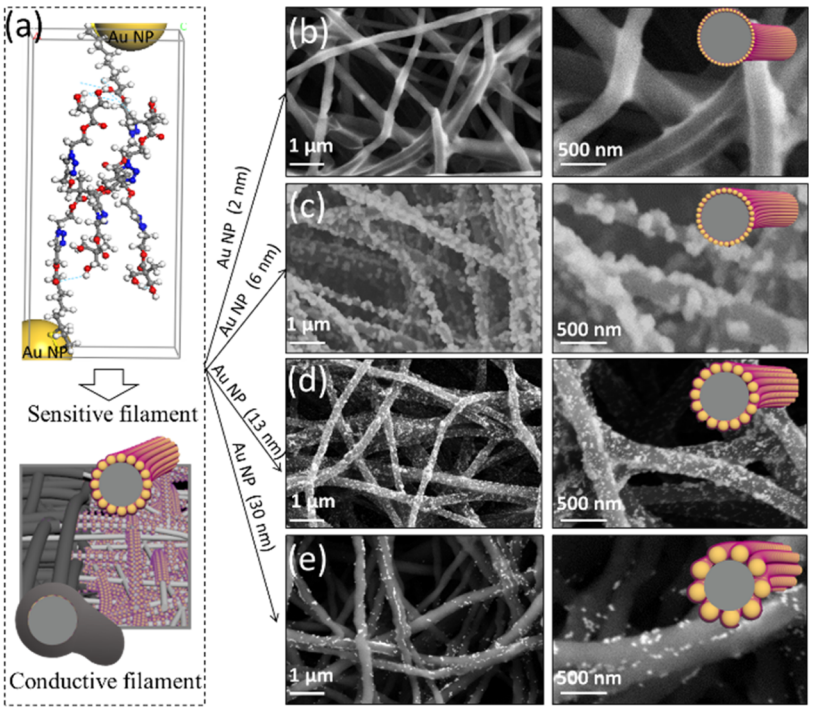

Figure 1. Illustration of nano-filaments with structurally sensitive dendrons and size-tunable Au NPs (a) and SEM images (b–e) of DD-AuNPs on PAN fibrous substrates with 2 (b), 6 (c), 13 (d), and 30 nm (e) NPs (see Figure S2 for the same fibrous substrates without NPs).

fine-tuning the intermolecular interactions, including −OH, −(C═O)−, −O−, and −N− sites. In contrast to the traditional 2D rigid sensing platform with functionalized nanoparticles, the 3D fibrous platforms enable a higher density of sensing sites with enhanced sensitivity.

2. EXPERIMENTAL METHODS

Synthesis of Dendrons. The dendrons were synthesized according to a previous paper.[11] The details are described in the Additional Information on Experimental Methods section and Figure S1 in the Supporting Information.

Synthesis of Au NPs. Au NPs with a diameter of 5 nm ($Au_{5\ nm}$) were prepared via a heat treatment of a solution of decanethiolate (DT)-Au_{2nm}, synthesized using Brust's two-phase method,[41] from room temperature to 150 °C. The final products in the suspension were cleaned with ethanol and acetone and centrifuged four times to remove solvents and possible byproducts. The final products showed an average size of 6.23 ± 0.33 nm. The synthesis of 13 and 30 nm Au NPs followed the methods described in our previous report.[11]

Preparation of the Dendronized Au NP Thin Film. The thin film was prepared by adding hydrophilic dendrons (deSG-SS) to the Au NP solution at a controlled ratio, where deSG-SS was anchored on the surface of DT-Au NPs via an "exchanging−crosslinking−precipitation" route.[41] An overnight time was allowed for the growth of the thin film.

Device Fabrication. The details for the microfabrication of the rigid/flat interdigitated microelectrodes (IMEs) were reported previously.[42] The IME devices, with 100 pairs of gold electrodes with a 200 μm length, a 10 μm width, and a 5 μm spacing on a 1 mm thick glass substrate (thickness of the Au electrodes: 100 nm), were fabricated via a standard microfabrication technique at the Cornell NanoScale Science and Technology Facility. The flexible/fibrous paper IME devices were fabricated using different types of papers, for example, two-layer [PAN/polyethylene terephthalate (PET)] membrane-type paper and Methode carbon ink, by printing the IMEs using an Optomec AJ-300 aerosol jet printer. Interdigitated carbon electrodes were printed using the diluted Methode ink in the ultrasonic atomizer and a 150 μm tip with a speed of 10 mm/s, and lines of 40 m were produced. The electrodes consist of 20 pairs of fingers which are 1.27 mm in length, 40 μm in width, and 40 μm in spacing and have 1.27 mm wide traces on each side. Printed electrodes were baked in an oven at 50 °C for 10 min following annealing. The final conductivity of the carbon-printed electrode was 50 kΩ/mm. The glass/gold and paper/carbon IME devices were then immersed into the solution of the dendronized Au NPs (DD-Au NPs), DT-Au NPs and NDT-Au NPs at room temperature, and solvent evaporation was prevented during the film formation. The thickness of the thin films grown on the surface of the substrates was controlled by immersion time. The thin films thus produced were thoroughly rinsed with the solvent and dried under nitrogen.

Sensor Measurement. The sensor devices were detected using a computer-interfaced multichannel multimeter (Keithley, model 2700). The IME devices were housed in a Teflon chamber with tubing connections to vapor gases and N_2 sources. The gas flow was controlled by a calibrated Aalborg mass flow controller (AFC-2600). N_2 was used as a reference gas and as a diluent to control the concentration of VOCs for a mixing ratio. The vapor concentration in the unit of parts per million (M) was determined from the partial vapor pressure and the mixing ratio of vapor and N_2 flows, which can be converted to parts per million (V) by multiplying by a factor of 24.5.[43]

Preparation of Fibrous PAN/PET and Poly(methyl methacrylate)/PET. The PAN/PET fibrous membrane substrates were prepared using a method described in a precious report.[44] Poly(methyl methacrylate) (PMMA)/PET fibrous substrates were prepared by electrospun deposition of PMMA fibers on a PET substrate. The preparation of PMMA followed a previous report[45] with a modification. Briefly, a PMMA polymer solution was prepared by dissolving PMMA in an organic solvent. The electrospinning process used a copper wire in the polymer solution, which was attached to the anode of the high-voltage power supply, and a metal cathode connected electrically to an aluminum foil as a collection screen. The PET support layer was attached on the top of the aluminum foil. Using a pipette tilted at approximately 10° from the horizontal, a small, viscous droplet was maintained at the capillary tip with a voltage of 20 kV (0.8 kV/cm) being applied at a distance of 25 cm between the polymer solution and the collection screen.

Characterizations. Infrared reflectance spectroscopy (IRS) spectra were acquired using a Nicolet 760 ESP Fourier transform infrared

https://doi.org/10.1021/acsami.2c00021
ACS Appl. Mater. Interfaces 2022, 14, 15391−15400

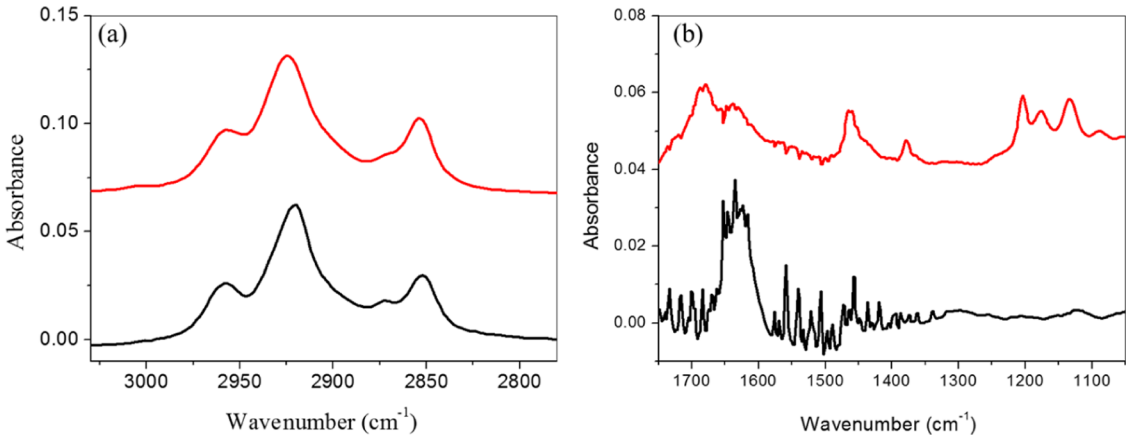

Figure 2. FTIR spectra of DT-AuNP (black) and DD-AuNP (red) filaments in 3050−2750 (a) and 1750−1150 cm^{-1} (b) ranges.

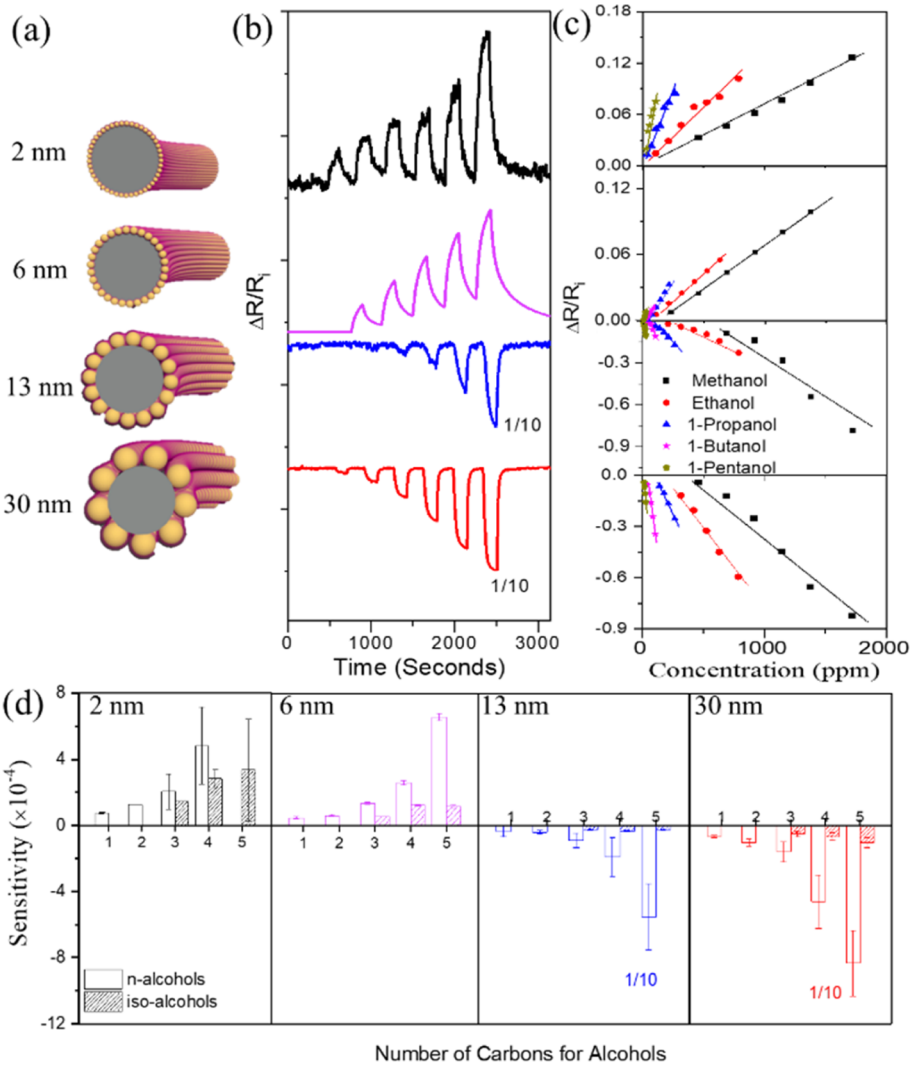

Figure 3. Response profiles and response sensitivities for the sensitive filaments with different Au NP sizes. (a) Illustration of the fibers with the Au NPs of different sizes (2, 6, 13, and 30 nm) crosslinked by dendrons as nano-filaments. (b) Response profiles to methanol vapors. (c) Responses to gaseous alcohols of different chain lengths and isomers in different concentrations. (d) Response sensitivities vs number of carbons in *n*-alcohols (empty bars) and iso-alcohols (filled bars). Note that the response (b) and sensitivity (d) of 13 and 30 nm are scaled by 1/10.

(FTIR) spectrometer with a liquid-nitrogen-cooled HgCdTe detector and an external reflection mode using *p*-polarized light at an incident angle of 82°. An octadecanethiolate-d_{37} monolayer on gold was used as the reference. A gold thin film on Cr-primed glass (Au/glass) was used as a substrate for the IRS measurement. NP thin films were cast onto the Au/glass substrate. The scanning electron microscopy (SEM) images were acquired using a field emission scanning electron microscope (Supra 55 VP from Zeiss) at 5 kV. The UV−visible spectra of the DD-

https://doi.org/10.1021/acsami.2c00021
ACS Appl. Mater. Interfaces 2022, 14, 15391−15400

Au NP thin film on the glass substrate were collected using an HP 8453 spectrophotometer over the range of 200−1100 nm.

Random Forest Classification and Principal Component Analysis. Statistical methods such as random forest (RF) classification and principal component analysis (PCA) were used to analyze the sensor array data. The relative standard deviation of the signal noises was considered in the analysis. The random noise data follow a normal distribution with a mean of zero and a standard deviation of 20% sample mean. RF is a classification method which provides feature importance.[46] A forest contains many decision trees, each of which is constructed with randomly sampled features. The output was computed by a majority vote of all decision trees. First, the overall node probability could be calculated as the number of samples that reach the node divided by the total number of samples. Next, feature importance was calculated by the product of decrease in node impurity (measured using the Gini Index)[47] and the overall node probability. The "RandomForestClassifier" algorithm in the Scikit-learn Python library was used to obtain feature importance. The inputs for the RF algorithm are noise-added sensor array responses from seven individual sensors. Lastly, the output of feature importance was used as criteria for feature selection of the sensor array. Higher values of feature importance imply more important features. Both before and after feature selection data were standardized before applying the PCA algorithm. PCA was used to analyze the data for the normal alcohols and their isomers. Good separations among different groups of the normal alcohols and their isomers serve as a promising indication of viability of the sensor array toward archiving high selectivity.

3. RESULTS AND DISCUSSION

3.1. Fabrication of the Nano-Filamented Fibrous Network. Figure 1 shows the assembly of the nano-filaments consisting of Au NPs and dendrons in electrospun polymeric fibrous substrates. In distinction to planar substrates, fibers feature highly curved surfaces. DD-Au NPs of different diameters (2, 6, 13, and 30 nm) were assembled via an "exchanging−crosslinking−precipitation" route (Figures 1a and S1). Based on the SEM images, an apparent difference is observed in terms of the nanoparticle aggregates or island formation on the fibers. It appears the tendency of forming aggregations or islands is higher as the particle size increases, which is believed to reflect the difference in nucleation and growth of the differently sized nanoparticles during the assembly process. For the assemblies of Au NPs of different sizes on PAN fiber substrates, PAN fiber@DD-Au NPs (2 nm) features a smooth thin film of Au NPs on fibers (Figure 1b). For DD-Au NPs (6 nm), the assembly yields aggregates wrapped over the PAN fiber surfaces (Figure 1c). In comparison, for DD-Au NPs of diameters 13 nm (Figure 1d) and 30 nm (Figure 1e), the assemblies showed the presence of NPs on the surface. The morphologies appear less continuous in comparison with that of the smaller-sized NPs, reflecting the operation of nucleation and growth for the nanoparticle assemblies on the surface of fibers during the assembly in the solution.

The dendron contains a disulfide functional group for anchorage to the gold surface and multiple sites for intermolecular hydrogen-bonding and van der Waals interactions, leading to the assembly of Au NPs as a thin film. The presence of dendrons in the assembly is evidenced by detection of the −C═O (1680 cm^{-1}) and C−O− (1100−1200 cm^{-1}) bands in the FTIR spectra (Figure 2), which are characteristic of ester and alcohol functional groups.

3.2. Chemical Responses of the Nano-Filamented Fibrous Network. IMEs (conductive filament) were embedded in the fibrous substrate as a chemiresistive element, which was followed by the assembly of DD-Au NPs as the sensing interface ((Figures 3a and S3a). One example involved carbon-printed IMEs as conductive filaments, as shown in Figure S3b, featuring 20 pairs of electrodes with a 1.2 mm finger length and a 40 μm finger gap. A fibrous paper substrate is derived from a custom-made paper with an electrospun PAN fibrous layer (fiber diameter: 163 ± 33 nm) (Figures S2 and S3c) with a thickness of about 80 μm and a nonwoven PET fibrous support layer (fiber diameter: 20 μm). The fibrous chemiresistive sensors in this work were prepared from the fibrous substrates with carbon-printed IMEs, followed by the assembly with DD-Au NPs of different diameters (2, 6, 13, and 30 nm) (sensitive nano-filaments). The cross-sectional view of the PAN fibrous substrate assembled with DD-Au NPs (13 nm) (Figure S3d) revealed dispersion of nanoparticle assemblies through the fibrous substrate.

As shown by the response profiles for methanol in Figure 3b using a sensor derived from DD-AuNPs on a fibrous paper substrate (PAN/PET), the absolute value of the sensing response is shown to increase with the nanoparticle sizes. The response profile is shown to switch from positive to negative as the nanoparticle size increases to 13 and 30 nm. Similar response characteristics were observed for other alcohols (Figures 3c, S4, and S5). As shown in Figure 3d for responses to n-alcohols and iso-alcohols, smaller nano-filaments display a lower sensitivity and positive response profile, while larger ones exhibit a higher sensitivity and negative response profile. Different response sensitivities between n-alcohols and iso-alcohols were also revealed. The data from the organic-synthesized Au NPs (6 nm) were compared with the data from the aqueous-synthesized Au NPs (6 nm) (Figure S6). Both showed positive response profiles and a similar chain length effect. This finding rules out the effect of different synthesis methods on sensing properties. The particle sizes played a key role in dictating the response profile.

The structure and response features of this type of sensor differ from those of previous chemiresistive sensors based on the thin film assembly of alkanethiolate-capped Au NPs, which produce largely positive response profiles resulting from the adsorption of VOCs, reflecting the resistance increase due to the interparticle distance increase upon the vapor sorption,[43] with a few exceptions. Examples include Au NP assembly with aromatic organo-thiol derivatives (HS−C_6H_4-X) of different functional groups (X) as crosslinkers, which show positive responses to methanol vapor for X = −OH and $-CH_3$ and negative responses for X = −COOH and $-NH_2$.[48] Alternative formulations include hydrogen-bonding-mediated assembly of Au NPs, which show negative responses to water and methanol but positive responses to ethanol, propanol, and so forth.[49] The Au−thiolate chemistry on the surface of gold enables the self-assembly of thiolate monolayers with different functional groups to tune the sensing interfaces.[50,51]

The fibrous sensors with different fiber diameters also include those derived from PAN fibers with a fiber diameter of 163 ± 33 nm and DD-Au NPs (6 nm), PMMA with a fiber diameter of 552 ± 99 nm and DD-Au NPs (6 nm), and carbon nanotubes (CNTs) with a diameter of 26 nm and 1,9-nonanedithiol (NDT)-capped Au (2 nm). PMMA was fabricated on the support of PET using an electrospinning method (Figure S7). The sensitivities were shown to increase with the number of carbons in the alcohols (Figure 4). For larger fiber diameters, a higher sensitivity was observed for longer-chain alcohols.

3.3. Origin of the High Structure Sensitivity of the Nano-Filamented Network. Considering the dielectric microenvironment in the sensitive nano-filaments, we believe

https://doi.org/10.1021/acsami.2c00021
ACS Appl. Mater. Interfaces 2022, 14, 15391−15400

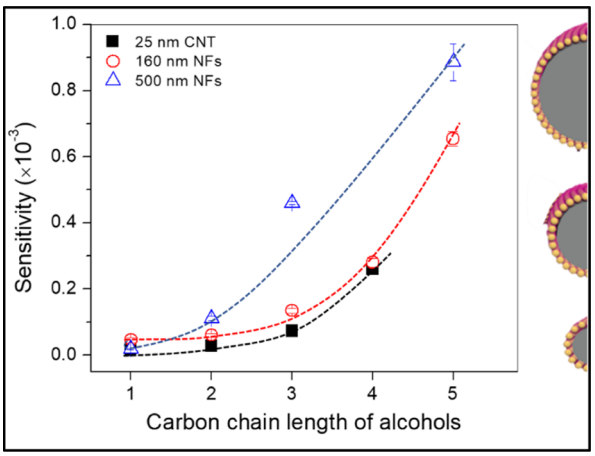

Figure 4. Plots of response sensitivity to different alcohols as a function of the chain length in terms of the number of carbons in alcohol molecules for the Au NPs in fibrous substrates with different fiber diameters (~25 nm for CNTs,[24] 163 ± 33 nm for PAN, and 552 ± 99 nm for PMMA).

that the origin of the positive−negative response profiles can be assessed from the two specific conditions: (1) the absence of strain in the assembly of NPs with different linkers on a flat substrate surface instead of the curved surface and (2) the presence of strain in the assembly of NPs on the fibers with different linkers. Figure 5a−c shows the variation of the interparticle distances and interactions by crosslinkers, including shorter DT and longer dendrons. For the first condition, Au NPs capped with DT were assembled by dendrons on a flat glass substrate printed with gold IMEs (Figure 5d). It shows methanol vapor response profiles for the assemblies of Au NPs

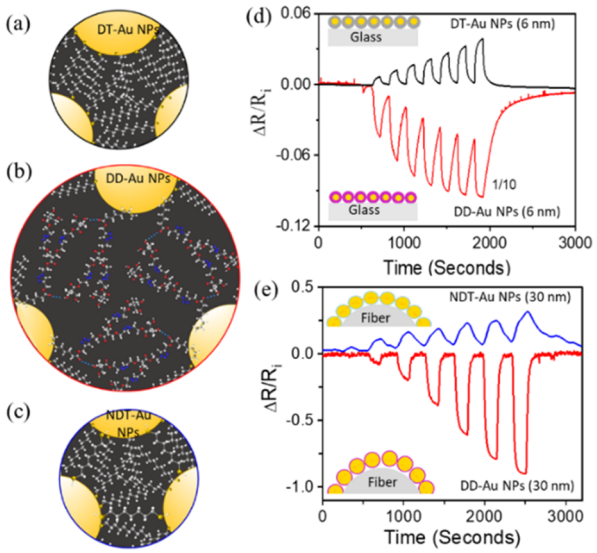

Figure 5. Illustrations of the different nano-filaments on IME-printed substrates and the corresponding response profiles. (a−c) Interparticle interactions with (a) DT, (b) dendrons, and (c) NDT linkers. (d) Response profiles to methanol vapors with sensitive filaments of DT-Au NPs (black) and DD-Au NPs (red) (6 nm) on an IME/glass substrate. Note that the response with DD-Au NPs is scaled by 1/10. (e) Response profiles to methanol vapors with sensitive filaments of NDT-Au NPs (blue) and DD-Au NPs (red) (30 nm) on an IME/fibrous substrate. The responses and sensitivities to different alcohols vs chain length are shown in Figure S8.

(6 nm) with DT and dendrons. In contrast to the positive response profile for DT-AuNPs, DD-AuNPs exhibit not only a negative response profile but also a 10 times higher magnitude. The response sensitivities clearly differ for different alcohols (Figures S8a and S9). The sensitivity increases with the alcohol chain length either in a positive (with DT) or negative direction (with dendrons) (Figure S8b). The differentiation between *n*-alcohols and *iso*-alcohols indicate lower sensitivity for *iso*-alcohols than that for *n*-alcohols, which show remarkable structure sensitivity.

The contribution of the second condition was assessed for the same set of alcohol vapors with assemblies of 30 nm Au NPs using various crosslinkers to create a different hydrophobic or hydrophilic balance, including NDT (a hydrophobic crosslinker) and dendrons (a hydrophilic crosslinker) at the presence of strain (Figures 5e and S8c,d). In the case of NDT, there is a hydrophobic microenvironment, and the dielectric constant of NDT is very small. There is a negative to positive change in the sensing profile when NDT is used as a crosslinker instead of larger-sized dielectric and hydrophilic dendrons. These findings demonstrate that the response characteristics depend on a combination of the nanoparticle size and capping/linking molecular properties of the sensitive filaments and the surface curvature of the fiber.

The results were further assessed by theoretical simulation, focusing on how the nanoparticle size, capping/linking molecule, and surface curvature influence the electron hopping and/or electron tunneling response (Figure S10). The dielectric constant of the surface and medium relate to the surface plasmon (SP) resonance of the nanoparticles. The blue shift of the simulated SP band upon switching from air to methanol is consistent with the experimental SP band evolution for DD-AuNPs (Figure S10a). Based on dielectric properties, the simulated sensitivity showed a good agreement with the experimental trend (Figure S10b), indicative of a change from a positive to negative response profile in a more hydrophilic microenvironment. Considering that the surface curvature introduced a positive change in thin film strain, the electrical response shows an increase in the positive direction (Figure S10c). Based on the dependence of thermally activated conductivity on interparticle distance and dielectric properties,[43] the sensitivity increases with the chain length of alcohols (Figure S10d), which agrees with the experimental result. While these results are qualitatively consistent with the simulated trends, a deep understanding of the detailed correlation with the experimental result requires further investigation of the changes in the film's interparticle distances and dielectric properties before and after the vapor adsorption.

3.4. Multiplexing of the Nano-Filamented Network Sensor Array. Given the above distinctive response characteristics depending on medium dielectric and fiber-curvature-induced interparticle strain properties, we further exploited their combination to design and construct an array with different nano-filaments as a proof-of-concept demonstration of the high structure sensitivity to alcohol molecules of different chain lengths and isomers (Figure 6). The sensor array is constructed from six individual sensors which are derived from different nano-filaments in terms of flat and fibrous substrates, NPs of different sizes, and linker molecules of different chemical natures, including those derived from 2D rigid DT-AuNPs (6 nm) and DD-AuNPs (6 nm) and 3D fibrous DD-AuNPs (2, 6, 13, and 30 nm) (Figure 6a,b).

https://doi.org/10.1021/acsami.2c00021
ACS Appl. Mater. Interfaces 2022, 14, 15391−15400

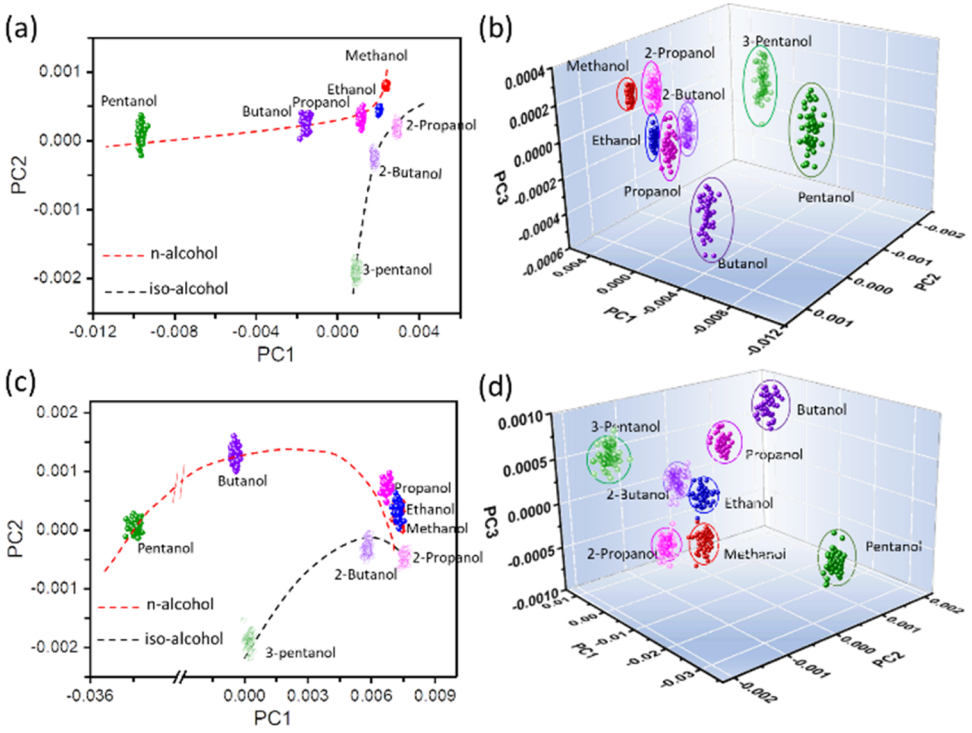

Figure 6. 2D and 3D PCA plots for the array responses to *n*-alcohols and their isomers: (a,b) array of six selected sensors with six different nano-filaments rigid [DT-AuNPs (6 nm), rigid DD-AuNPs (6 nm), and fibrous DD-AuNPs (2, 6, 13, and 30 nm)]. (c,d) Array of four feature-important sensors with four different nano-filaments rigid [DD-AuNPs (6 nm), fibrous DD-AuNPs (13 nm), DD-AuNPs (30 nm), and NDT-AuNPs (30 nm)].

Based on the PCA of the array's response sensitivities to alcohols of different chain lengths, the result showed high selectivity not only for the alcohols with varied chain lengths but also for the different isomers: *n*-alcohols and *iso*-alcohols. RandomForestClassifier was also used to analyze the sensing data for the sensors based on feature importance analysis (Figure S11). 2D rigid DD-Au NPs (6 nm), 3D fibrous DD-Au NPs (13 nm), DD-Au NPs (30 nm), and NDT-Au NPs (30 nm) were selected based on the importance of the feature parameters. The selected four-sensor array is shown to achieve the same level of separation of the alcohols (Figure 6c,d). The PCA results demonstrate the capability to separate the alcohols of different lengths, as shown by the gradual change in terms of PCA coordinates, and differentiate the normal alcohols and their isomers, as shown by the different locations in the PCA plot.

The demonstration of the multiplexing capability is significant considering the viability of the sensor array application in the detection of multiple isomeric alcohol VOCs in lung cancer breath or other biomarkers, such as 2-ethyl-1-hexanol, 2-ethyl-4-methyl-1-pentanol, and 2-propyl-1-pentanol, which is often difficult to differentiate[36] under high-humidity conditions. Traditional approaches for the detection of the blood alcohol content level involve blood sampling or urine monitoring, which are invasive or time-consuming. Saliva, breath, and sweat samples are convenient for noninvasive and real-time alcohol detection. Some of the reported sensors include 2D photonic crystals,[38] a titanium dioxide composite, or graphite-doped hydroxyapatite nanoceramics[39,40] for sensing methanol, ethanol, propanol, butanol, and propanol. However, most have a high false-positive rate due to the interference of the high moisture content and other compounds in the samples, and none of the noninvasive sensors, including commercial ones, have shown the ability for sensing alcohols with different chain lengths and isomers. The nano-filamented polymeric network arrays provide increased tunability of sensitivity and selectivity and show potential for application in breath sensing of alcohol VOC biomarkers of lung cancer and sensing of other biomarkers from sweat, both under high-humidity or -moisture conditions.

4. CONCLUSIONS

Taken together, we have demonstrated a fibrous sensor platform with high structure sensitivity by imparting fibrous networks with nano-filaments consisting of structurally sensitive dendrons and size-tunable Au NPs. The high structure sensitivity of the nano-filaments is shown to be tunable by the sizes of nanoparticles and fibers in terms of response profiles and sensitivities to alcohol molecules and their isomers. This tunability reflects not only the unique multisite characteristics of nanofilaments but also the subtle combination of the curvature strain of the fibers and the dielectric medium property of the nano-filaments in fibrous networks. The arrays constructed from different combinations of the filaments are shown to exhibit a clear increase as a function of the chain length of n-alcohols and iso-alcohols, a remarkably high structure sensitivity, which is to our knowledge the first example of the dendron−nanoparticle filament-enabled fibrous sensor platform. These findings have implications for a paradigm shift in the design of sensor and biosensor arrays with high structure sensitivity for monitoring human performance and air quality, which are part of our ongoing investigations. A key element of the findings is the tunability of the sensing properties to alcohol VOCs by a combination of the nano-filaments and the fiber sizes. In addition to the expected enhancement in lowering the detection limit, this tunability could increase the sensitivity and selectivity of the sensors to human breath and sweat alcohol levels. Currently, the most reliable detection of blood alcohol content levels involves blood sampling or urine monitoring,

https://doi.org/10.1021/acsami.2c00021
ACS Appl. Mater. Interfaces 2022, 14, 15391−15400

which are invasive or time-consuming.[37] Saliva, breath, and sweat samples are convenient for noninvasive and real-time alcohol detection in correlation with blood ethanol[52] and breath alcohols in lung cancer breath such as 2-ethyl-1-hexanol, 2-ethyl-4-methyl-1-pentanol, and 2-propyl-1-pentanol,[36] which have small differences structurally. The sensor arrays, upon further optimization of the preparation and the stability, may be integrated into wearable textile sensors in a mask or cloth for the targeted applications.

■ ASSOCIATED CONTENT

Supporting Information

The Supporting Information is available free of charge at https://pubs.acs.org/doi/10.1021/acsami.2c00021.

Additional experimental details, characterization results, polymer structures, sensor data, and simulation details (PDF)

■ AUTHOR INFORMATION

Corresponding Author

Chuan-Jian Zhong − *Department of Chemistry, State University of New York at Binghamton, Binghamton, New York 13902, United States;* orcid.org/0000-0003-0746-250X; Email: cjzhong@binghamton.edu

Authors

Shan Yan − *Department of Chemistry, State University of New York at Binghamton, Binghamton, New York 13902, United States*

Dong K. Dinh − *System Science and Industrial Engineering, State University of New York at Binghamton, Binghamton, New York 13902, United States*

Guojung Shang − *Department of Chemistry, State University of New York at Binghamton, Binghamton, New York 13902, United States*

Shan Wang − *Department of Chemistry, State University of New York at Binghamton, Binghamton, New York 13902, United States*

Wei Zhao − *Department of Chemistry, State University of New York at Binghamton, Binghamton, New York 13902, United States*

Xin Liu − *Department of Chemistry, State University of New York-ESF, Syracuse, New York 13210, United States*

Richard Robinson − *Department of Chemistry, State University of New York at Binghamton, Binghamton, New York 13902, United States*

Jack P. Lombardi, III − *System Science and Industrial Engineering, State University of New York at Binghamton, Binghamton, New York 13902, United States*

Ning He − *Department of Chemical and Biochemical Engineering, College of Chemistry and Chemical Engineering, Xiamen University, Xiamen 361005, China;* orcid.org/0000-0002-2698-877X

Susan Lu − *System Science and Industrial Engineering, State University of New York at Binghamton, Binghamton, New York 13902, United States*

Mark Poliks − *System Science and Industrial Engineering, State University of New York at Binghamton, Binghamton, New York 13902, United States;* orcid.org/0000-0003-3872-6037

Benjamin S. Hsiao − *Department of Chemistry, Stony Brook University, Stony Brook, New York 11794, United States;* orcid.org/0000-0002-3180-1826

Ivan Gitsov − *Department of Chemistry, State University of New York-ESF, Syracuse, New York 13210, United States;* orcid.org/0000-0001-7433-8571

Complete contact information is available at: https://pubs.acs.org/10.1021/acsami.2c00021

Notes

The authors declare no competing financial interest.

■ ACKNOWLEDGMENTS

This work was funded by the National Science Foundation (CHE 2102482; IIP 1640669). Support from the SUNY Network of Excellence Funds, Binghamton University IEEC, Harpur College Research Seed, and Watson-UHS Research Seed is also acknowledged.

■ REFERENCES

(1) Yang, B.; Xiong, Y.; Ma, K.; Liu, S.; Tao, X. Recent Advances in Wearable Textile-Based Triboelectric Generator Systems for Energy Harvesting from Human Motion. *EcoMat* **2020**, *2*, No. e12054.

(2) Koch, H. C.; Schmelzeisen, D.; Gries, T. 4d Textiles Made by Additive Manufacturing on Pre-Stressed Textiles—an Overview. *Actuators*; Multidisciplinary Digital Publishing Institute, 2021; Vol. *10*, p 31.

(3) Mitchell, A.; Lafont, U.; Hołyńska, M.; Semprimoschnig, C. Additive Manufacturing—a Review of 4d Printing and Future Applications. *Addit. Manuf.* **2018**, *24*, 606−626.

(4) Jiang, P.; Ji, Z.; Wang, X.; Zhou, F. Surface Functionalization−a New Functional Dimension Added to 3d Printing. *J. Mater. Chem. C* **2020**, *8*, 12380−12411.

(5) Li, Y.; Yang, F.; Yu, J.; Ding, B. Hydrophobic Fibrous Membranes with Tunable Porous Structure for Equilibrium of Breathable and Waterproof Performance. *Adv. Mater. Interfaces* **2016**, *3*, 1600516.

(6) Le, P. N.; Huynh, C. K.; Tran, N. Q. Advances in Thermosensitive Polymer-Grafted Platforms for Biomedical Applications. *Mater. Sci. Eng.: C* **2018**, *92*, 1016−1030.

(7) Lu, L.; Yang, B.; Liu, J. Flexible Multifunctional Graphite Nanosheet/Electrospun-Polyamide 66 Nanocomposite Sensor for Ecg, Strain, Temperature and Gas Measurements. *Chem. Eng. J.* **2020**, *400*, 125928.

(8) Luo, G.; Zhang, Q.; Li, M.; Chen, K.; Zhou, W.; Luo, Y.; Li, Z.; Wang, L.; Zhao, L.; Teh, K. S.; Jiang, Z. A Flexible Electrostatic Nanogenerator and Self-Powered Capacitive Sensor Based on Electrospun Polystyrene Mats and Graphene Oxide Films. *Nanotechnology* **2021**, *32*, 405402.

(9) Cheng, H.-W.; Yan, S.; Shang, G.; Wang, S.; Zhong, C.-J. Strain Sensors Fabricated by Surface Assembly of Nanoparticles. *Biosens. Bioelectron.* **2021**, *186*, 113268.

(10) Yan, S.; Shan, S.; Wen, J.; Li, J.; Kang, N.; Wu, Z.; Lombardi, J.; Cheng, H. W.; Wang, J.; Luo, J.; He, N.; Mott, D.; Wang, L.; Ge, Q.; Hsiao, B. S.; Poliks, M.; Zhong, C. J. Surface-Mediated Interconnections of Nanoparticles in Cellulosic Fibrous Materials toward 3d Sensors. *Adv. Mater.* **2020**, *32*, 2002171.

(11) Yan, S.; Liu, X.; Skeete, Z.; He, N.; Xie, Z. H.; Zhao, W.; Lombardi, J. P., III; Liu, K.; Kang, N.; Luo, J.; Hsiao, B. S.; Poliks, M.; Gitsov, I.; Zhong, C. J. Decoration of Nanofibrous Paper Chemiresistors with Dendronized Nanoparticles toward Structurally Tunable Negative-Going Response Characteristics to Human Breathing and Sweating. *Adv. Mater. Interfaces* **2017**, *4*, 1700380.

(12) Kang, N.; Lin, F.; Zhao, W.; Lombardi, J. P.; Almihdhar, M.; Liu, K.; Yan, S.; Kim, J.; Luo, J.; Hsiao, B. S.; Poliks, M.; Zhong, C.-J. Nanoparticle−Nanofibrous Membranes as Scaffolds for Flexible Sweat Sensors. *ACS Sens* **2016**, *1*, 1060−1069.

(13) Yin, J.; Hu, P.; Luo, J.; Wang, L.; Cohen, M. F.; Zhong, C.-J. Molecularly Mediated Thin Film Assembly of Nanoparticles on Flexible Devices: Electrical Conductivity Versus Device Strains in Different Gas/Vapor Environment. *ACS Nano* **2011**, *5*, 6516−6526.
(14) Zhao, W.; Rovere, T.; Weerawarne, D.; Osterhoudt, G.; Kang, N.; Joseph, P.; Luo, J.; Shim, B.; Poliks, M.; Zhong, C.-J. Nanoalloy Printed and Pulse-Laser Sintered Flexible Sensor Devices with Enhanced Stability and Materials Compatibility. *ACS Nano* **2015**, *9*, 6168−6177.
(15) Shan, S.; Zhao, W.; Luo, J.; Yin, J.; Switzer, J. C.; Joseph, P.; Lu, S.; Poliks, M.; Zhong, C.-J. Flexibility Characteristics of a Polyethylene Terephthalate Chemiresistor Coated with a Nanoparticle Thin Film Assembly. *J. Mater. Chem. C* **2014**, *2*, 1893−1903.
(16) Clifford, A.; Das, J.; Yousefi, H.; Mahmud, A.; Chen, J. B.; Kelley, S. O. Strategies for Biomolecular Analysis and Continuous Physiological Monitoring. *J. Am. Chem. Soc.* **2021**, *143*, 5281−5294.
(17) Li, Z.; Wang, J.; Dai, L.; Sun, X.; An, M.; Duan, C.; Li, J.; Ni, Y. Asymmetrically Patterned Cellulose Nanofibers/Graphene Oxide Composite Film for Humidity Sensing and Moist-Induced Electricity Generation. *ACS Appl. Mater. Interfaces* **2020**, *12*, 55205−55214.
(18) Feiner, R.; Dvir, T. Soft and Fibrous Multiplexed Biosensors. *Nat. Biomed. Eeng.* **2020**, *4*, 135−136.
(19) Ma, L.; Wu, R.; Miao, H.; Fan, X.; Kong, L.; Patil, A.; Liu, X. Y.; Wang, J. All-in-One Fibrous Capacitive Humidity Sensor for Human Breath Monitoring. *Text. Res. J.* **2021**, *91*, 398−405.
(20) Petropoulou, A.; Kralj, S.; Karagiorgis, X.; Savva, I.; Loizides, E.; Panagi, M.; Krasia-Christoforou, T.; Riziotis, C. Multifunctional Gas and Ph Fluorescent Sensors Based on Cellulose Acetate Electrospun Fibers Decorated with Rhodamine B-Functionalised Core-Shell Ferrous Nanoparticles. *Sci. Rrep.* **2020**, *10*, 1−14.
(21) Sharma, P. R.; Sharma, S. K.; Lindström, T.; Hsiao, B. S. Nanocellulose-Enabled Membranes for Water Purification: Perspectives. *Adv. Sustain. Syst.* **2020**, *4*, 1900114.
(22) Zhou, J.; Miles, R. N. Sensing Fluctuating Airflow with Spider Silk. *Proc. Natl. Acad. Sci.* **2017**, *114*, 12120−12125.
(23) Xu, S.; Jung, I. H.; Rogers, J. A. Functional Fabric Devices Having Integrated Sensors. Google Patent WO 2018209100 A1, 2021.
(24) Ballard, Z. S.; Joung, H. A.; Goncharov, A.; Liang, J.; Nugroho, K.; Di Carlo, D.; Garner, O. B.; Ozcan, A. Deep Learning-Enabled Point-of-Care Sensing Using Multiplexed Paper-Based Sensors. *NPJ Digit. Med.* **2020**, *3*, 66.
(25) Biswas, S. K.; Chatterjee, S.; Bandyopadhyay, S.; Kar, S.; Som, N. K.; Saha, S.; Chakraborty, S. Smartphone-Enabled Paper-Based Hemoglobin Sensor for Extreme Point-of-Care Diagnostics. *ACS Sens* **2021**, *6*, 1077−1085.
(26) Zhao, W.; Al-Nasser, L. F.; Shan, S.; Li, J.; Skeete, Z.; Kang, N.; Luo, J.; Lu, S.; Zhong, C.-J.; Grausgruber, C. J.; Harris, R. Detection of Mixed Volatile Organic Compounds and Lung Cancer Breaths Using Chemiresistor Arrays with Crosslinked Nanoparticle Thin Films. *Sens. Actuators B Chem.* **2016**, *232*, 292−299.
(27) Shrivas, K.; Monisha, T.; Kant, T.; Karbhal, I.; Kurrey, R.; Sahu, B.; Sinha, D.; Patra, G. K.; Deb, M. K.; Pervez, S. Smartphone Coupled with Paper-Based Chemical Sensor for on-Site Determination of Iron (Iii) in Environmental and Biological Samples. *Anal. Bioanal. Chem* **2020**, *412*, 1573−1583.
(28) Wang, H.; Vagin, S. I.; Rieger, B.; Meldrum, A. An Ultrasensitive Fluorescent Paper-Based CO_2 Sensor. *ACS Appl. Mater. Interfaces* **2020**, *12*, 20507−20513.
(29) Yang, G.; Fang, X.; Jia, Q.; Gu, H.; Li, Y.; Han, C.; Qu, L. L. Fabrication of Paper-Based Sers Substrates by Spraying Silver and Gold Nanoparticles for Sers Determination of Malachite Green, Methylene Blue, and Crystal Violet in Fish. *Mikrochim. Acta* **2020**, *187*, 310.
(30) Rafatmah, E.; Hemmateenejad, B. Dendrite Gold Nanostructures Electrodeposited on Paper Fibers: Application to Electrochemical Non-Enzymatic Determination of Glucose. *Sens. Actuators B Chem.* **2020**, *304*, 127335.
(31) Liu, Z.; Zhou, C.; Zheng, B.; Qian, L.; Mo, Y.; Luo, F.; Shi, Y.; Choi, M. M. F.; Xiao, D. In Situ Synthesis of Gold Nanoparticles on Porous Polyacrylonitrile Nanofibers for Sensing Applications. *Analyst* **2011**, *136*, 4545−4551.
(32) Cheng, D.; Bai, X.; Pan, J.; Wu, J.; Ran, J.; Cai, G.; Wang, X. In Situ Hydrothermal Growth of Cu Nps on Knitted Fabrics through Polydopamine Templates for Heating and Sensing. *Chem. Eng. J.* **2020**, *382*, 123036.
(33) Li, S.; Liu, H. Q.; Liu, L.-H.; LiN, Q.; Zhai, X. Effect of Silver Film Thickness on the Surface Plasma Resonance in the Rectangular Ag-Si-SiO_2 Cavity. *J. Phys. Commun* **2018**, *2*, 055024.
(34) Shahzamani, Z.; Ranjbar, M.; Comini, E.; Goodarzi, M. T.; Salamati, H.; Sberveglieri, G. Palladium Thin Films on Microfiber Filtration Paper as Flexible Substrate and Its Hydrogen Gas Sensing Mechanism. *Int. J. Hydrog.* **2019**, *44*, 17185−17194.
(35) Tan, L.; Tan, B. Hypercrosslinked Porous Polymer Materials: Design, Synthesis, and Applications. *Chem. Soc. Rev.* **2017**, *46*, 3322−3356.
(36) Broza, Y. Y.; Zhou, X.; Yuan, M.; Qu, D.; Zheng, Y.; Vishinkin, R.; Khatib, M.; Wu, W.; Haick, H. Disease Detection with Molecular Biomarkers: From Chemistry of Body Fluids to Nature-Inspired Chemical Sensors. *Chem.Rev.* **2019**, *119*, 11761−11817.
(37) Oktivasari, P.; Ramadhan, F. A Low-Cost Design of Urine Detector. *iCAST*; IEEE, 2018; pp 458−463.
(38) Mehdi, G.; Hocini, A. Design of Bio-Alcohol Sensor Based on Two-Dimensional Photonic Crystal in a Nanophotonic Structure. *ICAEE*; IEEE, 2019; pp 1−6.
(39) Taha, S.; Begum, S.; Narwade, V. N.; Halge, D. I.; Dadge, J. W.; Mahabole, M. P.; Khairnar, R. S.; Bogle, K. A. Development of Alcohol Sensor Using Tio2-Hydroxyapatite Nano-Composites. *Mater. Chem. Phys.* **2020**, *240*, 122228.
(40) Taha, S.; Begum, S.; Narwade, V. N.; Halge, D. I.; Dadge, J. W.; Mahabole, M. P.; Khairnar, R. S.; Bogle, K. A. Enhancing Alcohol Sensing Properties of Hydroxyapatite Via Synthesis of Its Composite with Tio2 Nano-Tube. *Appl. Phys. A* **2021**, *127*, 1−9.
(41) Leibowitz, F. L.; Zheng, W.; Maye, M. M.; Zhong, C.-J. Structures and Properties of Nanoparticle Thin Films Formed Via a One-Step Exchange− Cross-Linking− Precipitation Route. *Analyt. Chem.* **1999**, *71*, 5076−5083.
(42) Wang, L.; Kariuki, N.; Schadt, M.; Mott, D.; Luo, J.; Zhong, C.-J.; Shi, X.; Zhang, C.; Hao, W.; Lu, S.; Kim, N.; Wang, J.-Q. Sensing Arrays Constructed from Nanoparticle Thin Films and Interdigitated Microelectrodes. *Sensors* **2006**, *6*, 667−679.
(43) Wang, L.; Shi, X.; Kariuki, N. N.; Schadt, M.; Wang, G. R.; Rendeng, Q.; Choi, J.; Luo, J.; Lu, S.; Zhong, C.-J.; Zhong, C. J. Array of Molecularly Mediated Thin Film Assemblies of Nanoparticles: Correlation of Vapor Sensing with Interparticle Spatial Properties. *J. Am. Chem. Soc.* **2007**, *129*, 2161−2170.
(44) Ma, H.; Yoon, K.; Rong, L.; Mao, Y.; Mo, Z.; Fang, D.; Hollander, Z.; Gaiteri, J.; Hsiao, B. S.; Chu, B. High-Flux Thin-Film Nanofibrous Composite Ultrafiltration Membranes Containing Cellulose Barrier Layer. *J. Mater. Chem.* **2010**, *20*, 4692−4704.
(45) Dong, H.; Nyame, V.; MacDiarmid, A. G.; Jones, W. E., Jr Polyaniline/Poly (Methyl Methacrylate) Coaxial Fibers: The Fabrication and Effects of the Solution Properties on the Morphology of Electrospun Core Fibers. *J. Polym. Sci. B Polym. Phys.* **2004**, *42*, 3934−3942.
(46) Breiman, L. Random Forests. *Machine Learning* **2001**, *45*, 5−32.
(47) Lerman, R. I.; Yitzhaki, S. A Note on the Calculation and Interpretation of the Gini Index. *Economics Letters* **1984**, *15*, 363−368.
(48) Evans, S. D.; Johnson, S. R.; Cheng, Y. L.; Shen, T. Vapour Sensing Using Hybrid Organic−Inorganic Nanostructured Materials. *J. Mater. Chem.* **2000**, *10*, 183−188.
(49) Han, L.; Daniel, D. R.; Maye, M. M.; Zhong, C.-J. Core− Shell Nanostructured Nanoparticle Films as Chemically Sensitive Interfaces. *Analyt. Chem.* **2001**, *73*, 4441−4449.
(50) Cheng, H.-W.; Wang, S.; Porter, M. D.; Zhong, C.-J. Molecularly-Tunable Nanoelectrode Arrays Created by Harnessing Intermolecular Interactions. *Chem. Sci.* **2021**, *12*, 6081−6090.
(51) Cheng, H.-W.; Wu, Z.-P.; Yan, S.; Li, J.; Shan, S.; Wang, L.; Porter, M. D.; Zhong, C.-J. A Simple Vaporous Probe with Atomic-

https://doi.org/10.1021/acsami.2c00021
ACS Appl. Mater. Interfaces 2022, 14, 15391−15400

Scale Sensitivity to Structural Ordering and Orientation of Molecular Assembly. *Chem. Sci.* **2019**, *10*, 7104−7110.
(52) Buono, M. J. Sweat Ethanol Concentrations Are Highly Correlated with Co-Existing Blood Values in Humans. *Exp. Physiol.* **1999**, *84*, 401−404.

https://doi.org/10.1021/acsami.2c00021
ACS Appl. Mater. Interfaces 2022, 14, 15391−15400